JACS
JOURNAL OF THE AMERICAN CHEMICAL SOCIETY



Article

# Unusual and Tunable Negative Linear Compressibility in the Metal–Organic Framework MFM-133(M) (M = Zr, Hf)

Yong Yan, Alice E. O'Connor, Gopikkaa Kanthasamy, George Atkinson, David R. Allan, Alexander J. Blake, and Martin Schröder

*J. Am. Chem. Soc.*, **Just Accepted Manuscript** • DOI: 10.1021/jacs.7b11747 • Publication Date (Web): 02 Feb 2018



## Just Accepted



ACS Publications

Journal of the American Chemical Society is published by the American Chemical Society. 1155 Sixteenth Street N.W., Washington, DC 20036

# Unusual and Tunable Negative Linear Compressibility in the Metal–Organic Framework MFM-133(M) (M = Zr, Hf)

Yong Yan,[1†] Alice E. O'Connor,[2†] Gopikkaa Kanthasamy,[2†] George Atkinson,[2] David R. Allan,[3] Alexander J. Blake,[2]* Martin Schröder[1]*

1. School of Chemistry, University of Manchester, Oxford Road, Manchester, M13 9PL, United Kingdom.

M.Schroder@manchester.ac.uk

2. School of Chemistry, University of Nottingham, University Park, Nottingham, NG7 2RD, United Kingdom.

A.J.Blake@nottingham.ac.uk

3. Diamond Light Source, Harwell Science and Innovation Campus, Didcot, Oxfordshire, OX11 0DE, United Kingdom.

[†]These authors contributed equally to this work.

**Abstract**

High pressure single-crystal X-ray structural analyses of isostructural MFM-133(M) (M = Zr, Hf) of **flu** topology and incorporating the tetracarboxylate ligand $TCHB^{4-}$ [$H_4TCHB$ = 3,3',5,5'-tetrakis(4-carboxyphenyl)-2,2',4,4',6,6'-hexamethyl-1,1'-biphenyl] and $\{M_6(\mu\text{-}OH)_8(OH)_8(COO)_8\}$ clusters, confirm negative linear compressibility (NLC) behavior along the *c* axis. This occurs *via* a three-dimensional wine-rack NLC mechanism leading to distortion of the octahedral cage towards a more elongated polyhedron under static compression. Despite the isomorphous nature of these two structures, MFM-133(Hf) shows a higher degree of NLC than the Zr(IV) analogue. Thus, for the first time, we demonstrate here that the NLC property can be effectively tuned in a framework material by simply varying the inorganic component of the frameworks without changing the network topology and structure.

## Introduction

Metal-organic frameworks (MOFs) are a class of porous materials constructed from inorganic ions/clusters bridged by organic linkers. Due to their high crystallinity the structures of these materials can often be accurately monitored by crystallographic methods[1] as a function of various external stimuli such as temperature and pressure.[2] Some MOFs undergo processes such as pressure-induced phase transitions[2b,3] and amorphization[4] when exposed to high pressures. The mechanisms for these pressure-induced structural behaviors need to be fully understood before such materials can be considered for practical applications. Although most materials contract in all dimensions under hydrostatic compression, others contract in one direction but expand in one or more directions, a rare phenomenon known as negative linear compressibility (NLC).[5,6] Only a limited number of materials have been reported to exhibit NLC, the majority of which are inorganic species such as $LaNbO_4$[7] and elemental Se.[8] A few molecular frameworks such as methanol monohydrate[9] and metallocyanides such as $Ag_3[Co(CN)_6]$[10] and $KMn[Ag(CN)_2]_3$[11] exhibit NLC properties, but this is extremely rare for MOFs.[12] Materials with NLC properties can find widespread use in high-pressure environments such as deep-sea optical telecommunications devices and piezo responsive devices (*i.e.*, highly sensitive pressure sensors,[13] smart body armor and shock-absorbing materials).[14]

MOF-5[15] and ZIF-8[16] have been studied using *in situ* single-crystal diffraction techniques under hydrostatic pressure. Although these materials show structural changes associated with the penetration of guest molecules of the pressure-transmitting medium into the pores under high pressure, they do not show NLC behavior. Frameworks displaying NLC are generally associated with specific network topologies featuring "wine-rack" and honeycomb-like structural motifs.[5,17] One well-known example is the MIL-53 family, which exhibits an extremely high degree of NLC, with a compressibility $K_{NLC} = -28$ $TPa^{-1}$ over 0–3 GPa.[18] Recently, a $\beta$-quartz-like framework $[InH(BDC)_2]$ ($H_2BDC$ = benzene-1,4-dicarboxylic acid) has been reported to exhibit an extreme NLC ($-62.4$ $TPa^{-1}$) involving a framework hinging mechanism.[19] The NLC behaviour of both the above examples correlates with the structural flexibility originating from the system of rigid elements connected by hinges.[20] The organic linkers provide another source of flexibility: frameworks employing large organic struts tend to show some degree of flexibility,[21] but frameworks with both rigid linkers and rigid inorganic clusters should intuitively be rigid in the absence of framework hinging.

Herein we show that two rigid frameworks MFM-133(M) (M = Zr, Hf) constructed from a rigid tetracarboxylate linker (Figure 1) and $\{M_6(\mu\text{-}OH)_8(OH)_8(COO)_8\}$ clusters exhibit unusual NLC behavior,

featuring the first examples of porous Zr(IV) and Hf(IV)-based MOFs displaying NLC. Despite the isomorphous nature of these two structures, MFM-133(Hf) shows a higher degree of NLC than the Zr(IV) analogue. By analyzing the high pressure crystallographic data, we reveal the mechanisms behind the different NLC behaviors of these two frameworks, and thus, for the first time, we have demonstrated an example of using crystal engineering methods to tune the NLC properties of frameworks materials without altering the underlying topology and structure.

**Results and Discussion**

Solvothermal reaction of $H_4$TCHB [3,3',5,5'-tetrakis(4-carboxyphenyl)-2,2',4,4',6,6'-hexamethyl-1,1'-biphenyl] with $ZrCl_4$ or $HfCl_4$ in DEF (diethyl formamide) at 120 °C in the presence of benzoic acid as modulator afforded single crystals of MFM-133(Zr) and MFM-133(Hf), respectively. Single-crystal X-ray diffraction revealed that these two materials are isomorphous, crystallizing in the tetragonal space group *P*4/*mnc*. MFM-133(Zr) contains the 8-connected octahedral $\{Zr_6(\mu\text{-}OH)_8(OH)_8(COO)_8\}$ cluster (Figure 1), which is observed in other Zr-based frameworks.[22] The methyl groups in the central part of $TCHB^{4-}$ enforce a twist of almost 90° between the two central mesitylene rings, resulting in a tetrahedral disposition of the carboxylate groups of the linker. Each linker is thereby connected to four $\{Zr_6\}$ clusters in a tetrahedral fashion and the whole framework forms a neutral (4,8)-connected network with fluorite (**flu**) topology.[23] An axially-elongated octahedral cage, with a cavity of diameter 10.4×10.4×25.9 Å, is constructed from eight $TCHB^{4-}$ units residing on the faces of the polyhedron and six $\{Zr_6\}$ clusters on the vertices. The solvent-accessible void volume for MFM-133(Zr) was calculated to be 71% using PLATON SOLV,[24] indicating its significantly porous structure. Due to the similar sizes of $\{Hf_6\}$ and $\{Zr_6\}$ clusters, MFM-133(Hf) shows very similar structural features to MFM-133(Zr) including the same degree of porosity.

High-pressure single crystal X-ray diffraction experiments were performed using a diamond anvil cell (DAC)[25] (see Supporting Information). Before loading a crystal into the DAC, residual DEF solvent from the synthesis was fully exchanged with 4:1 MeOH/EtOH which was used as the pressure transmitting medium. For MFM-133(Zr), diffraction data were collected at 293 K on one single crystal at pressures ranging from ambient up to 4.41 GPa. The variation of lattice parameter values as a function of pressure is shown in Figure 2. It is immediately apparent that upon compression the equivalent *a* and *b* axes contract in length, but the *c* axis expands. Over the pressure range studied, lattice parameter *a* and the unit cell volume decrease by

0.628(5) Å (3.2 %) and 521(6) Å$^3$ (4.2 %), respectively, whilst lattice parameter *c* increases by 0.732(8) Å (2.2 %). The data were fitted using an empirical equation $l = l_0 + \lambda(p - p_c)^v$ ,[26] giving the linear compressibilities along *a* (or *b*) and *c* as 5.9 and –5.1 TPa$^{-1}$, respectively, over the pressure range 0–4.4 GPa. The value of NLC of –5.1 TPa$^{-1}$ is higher than for other molecular frameworks such as $[NH_4][Zn(HCOO)_3]$ ($K_{NLC}$ = –1.8 TPa$^{-1}$)[27] and ZAG-4 ($K_{NLC}$ = –2.6 TPa$^{-1}$),[3] but lower than metallocyanide frameworks $Ag_3[Co(CN)_6]$-I ($K_{NLC}$ = –76 TPa$^{-1}$)[10] and $KMn[Ag(CN)_2]_3$ ($K_{NLC}$ = –12 TPa$^{-1}$),[11] indicating moderately strong NLC behavior for MFM-133(Zr). The pressure dependence of the unit cell volume has been analyzed using a second-order Birch-Murnaghan equation of state (see Supporting Information)[28] to give a value for the bulk moduli *B* of 88.7 GPa (0–2 GPa), which is higher than for most other framework materials.[6] However, this value is significantly lower than the bulk moduli for the Zr materials UiO-67 (174 GPa) and UiO-abdc (580 GPa)[29] over the same pressure range 0–2 GPa, reflecting the relative softness of MFM-133(Zr).

The reversibility of the NLC shown by MFM-133(Zr) was also assessed by collecting diffraction data upon sequential release of pressure to 2.76, 2.09 and 1.03 GPa. Indeed, the decompression results reveal that the NLC is fully reversible, with the lattice parameter *a* increasing from 19.016(3) Å at 4.41 GPa to 19.642(6) Å at 1.03 GPa, and *c* decreasing from 33.102(8) Å at 4.41 GPa to 32.94(10) Å at 1.03 GPa. The unit cell volume also increases during decompression [11970(4) Å$^3$ at 4.41 GPa to 12708(38) Å$^3$ at 1.03 GPa]. This further confirms that flexibility and stability of this framework material, which is the important requirement for a material to find practical applications in high-pressure environments.

In order to understand the mechanism underlying the NLC in MFM-133(Zr) at a molecular level, we undertook an analysis of the structural changes under compression by constructing an octahedron with its vertices at the centroids of six $\{Zr_6(\mu\text{-}OH)_8(OH)_8(COO)_8\}$ clusters. The octahedron can also be visualized as two identical rhombi sharing two axial vertices in a perpendicular fashion (Figure 3a). Thus, two angles θ and δ can be used to define the shape of these rhombi (Figure 3b). When the pressure is increased, θ decreases from 80.4° at 0.95 GPa to 78.1° at 4.28 GPa, a decrease of 2.9%, while δ increases by 2.4% over the same pressure range, from 49.8° to 51.0°. The ratio of the two diagonal axes of the rhombus ($L_1/L_2$, Figure 3b) also increases from 1.18 at 0.95 GPa to 1.23 at 4.28 GPa. Examination of the relevant bond distances and angles indicates that the geometry of the $\{Zr_6\}$ inorganic cluster is unaffected by pressure. The decrease in θ and increase in δ and the ratios of diagonal axes of the rhombi under compression is

reminiscent of the mechanism of the "wine-rack" motif, where the organic linkers act as rigid struts, while the inorganic clusters act as framework hinges. However, the framework of MFM-133(Zr) is different from the two-dimensional wine-rack topology shown by molecular networks such as MIL-53,[18] where contraction only affects one dimension of the crystal lattice. MFM-133(Zr) contracts in two dimensions, resulting in the octahedral cage being distorted into a more elongated polyhedron (with increased ratio of the diagonal axes of 1.23 at 4.28 GPa compared to 1.18 at 0.95 GPa) under static compression.

A close examination of the conformation of the organic linker within the whole pressure range shows that the dihedral angle between the two central mesitylene rings in MFM-133(Zr) lies in the range 79–89°, but does not follow a significant trend with increasing pressure. The limited variation of this dihedral angle indicates that there is restricted freedom of rotation between the central mesitylene rings. However, the relatively large octahedral cage is comprised of eight $TCHB^{4-}$ units. Therefore, the effect of the limited flexibility shown by one linker can by amplified, resulting in more noticeable flexibility observed for the overall structure.

The response of single crystals of MFM-133(Hf) to static pressures of up to 4.9 GPa at 293 K was analyzed using the same experimental methods as were applied for MFM-133(Zr). MFM-133(Hf) reveals the same NLC behavior as the Zr(IV) analogue, with contraction along the *a* and *b* axes, expansion along the *c* axis, and a continuous decrease in unit cell volume with increasing pressure (Figure 4). The lattice parameters at different pressures were fitted using the same empirical equation $l = l_0 + \lambda(p - p_c)^{v}$[26] as for MFM-133(Zr) (see Supporting Information). The lattice parameters *a* (or *b*) and *c* in MFM-133(Hf) show a gradual respective decrease and increase with increasing pressure up to 4.9 GPa. This change in lattice parameters is different from that in MFM-133(Zr), where the changes in *a* (or *b*) and *c* reach a plateau in the high pressure region 3.5–4.5 GPa, indicating that the framework of MFM-133(Zr) becomes significantly harder and cannot be further deformed with increasing pressure. Up to 3 GPa, the lattice parameters for both frameworks show similar decreases; however, above 3 GPa MFM-133(Hf) reveals slightly larger changes in lattice parameters: *e.g.*, by 4 GPa, the shrinkage in *a* is 4.3% [*cf.* 3.2% for MFM-133(Zr)], and the expansion in *c* is 3.8% [*cf.* 2.4% for MFM-133(Zr)]. Empirical fitting of the pressure-dependent lattice parameters gives compressibility values of 10.7 $TPa^{-1}$ for *a*/*b* and –7.9 $TPa^{-1}$ for *c* over the pressure range of 0–4.9 GPa, indicating that MFM-133(Hf) shows higher degree of NLC than the Zr(IV) analogue. Significantly, by 4.9

GPa, the *a* (or *b*) axis in MFM-133(Hf) has contracted by 6.5% compared to its starting value at ambient pressure, while the *c* axis has increased by 5.5%. The bulk modulus of MFM-133(Hf) was estimated using a second-order Birch−Murnaghan equation of state (Fig. S11) to give a value for $B_0$ of 44.8 GPa, lower than that of MFM-133(Zr).

The NLC in MFM-133(Hf) involves the same mechanism as in its Zr(IV) analogue, which is unsurprising given the isostructural nature of these two frameworks. Compared with the $\{Zr_6\}$ cluster, the $\{Hf_6(\mu\text{-}OH)_8(OH)_8(COO)_8\}$ unit is slightly smaller due to the shorter Hf–O (COO) bond lengths within the studied pressure range (Hf1–O_A: 2.11–2.19 Å; Zr1–O_A: 2.22–2.28 Å; Hf2–O_B: 2.1–2.16; Zr2–O_B: 2.15–2.21, Fig. S7) and is also unaffected by compression. Therefore, the flexibility of the octahedral cage comprising six $\{Hf_6\}$ clusters and eight $TCHB^{4-}$ units is largely attributable to the flexibility of the organic linkers which in turn arises from the twisted geometry of the two connected mesitylene rings in the $TCHB^{4-}$ units. The dihedral angle between these two central mesitylene rings in MFM-133(Hf) lies in the range 70–80° above 1.5 GPa, which is about 10° lower than that in MFM-133(Zr), indicating the two central mesitylene rings in the $L^{4-}$ in MFM-133(Hf) are less twisted than in the Zr(IV) structure in the higher pressure region (1.5–4 GPa). At the highest pressure studied for MFM-133(Hf) (4.9 GPa), this angle reaches 71.2°, resulting in a very short C•••C distance of 2.79 Å between the adjacent methyl groups on the two central mesitylene rings. The less twisted geometry of the mesitylene rings in MFM-133(Hf) makes the linker unit lie flatter, bringing the equatorial $\{Hf_6\}$ clusters in the octahedral cage closer and pushing the two axial $\{Hf_6\}$ clusters further apart, thus resulting overall in a larger NLC effect (Fig. S7).

**Conclusions**

In summary, two isomorphous framework materials MFM-133(M) (M = Hf, Zr) have been synthesized by employing a tetracarboxylic acid containing two central mesitylene rings and a twisted geometry within the linker. The inorganic component of the framework consists of octahedral $\{M_6(\mu\text{-}OH)_8(OH)_8(COO)_8\}$ (M = Zr, Hf) clusters. The $TCHB^{4-}$ unit exhibits a tetrahedral disposition of its four carboxylate groups, resulting in a rare **flu** topology for these frameworks. Both frameworks reveal unusual negative linear compressibility, where under static pressure contraction of the *a* and *b* axes is accompanied by expansion of the *c* axis. This is the first observation of NLC behavior in molecular frameworks of **flu** topology and these two materials are among limited examples of porous molecular structures showing NLC. The NLC in MFM-133(M) (M = Zr,

Hf) follows a "wine-rack" mechanism where the octahedral clusters and eight $TCHB^{4-}$ linkers contract equatorially and expand axially. MFM-133(Hf) reveals larger linear compressibilities in all three directions than MFM-133(Zr) over the pressure range studied (0–4.9 GPa). Thus, we demonstrate that the NLC in materials can be effectively tuned by simply varying the inorganic component of the framework. It is anticipated that the high-pressure studies on MFM-133(M) (M = Zr, Hf) and the resulting knowledge of the mechanism by which NLC occurs, will lead to the exploitation of such NLC materials in various applications such as pressure sensitive sensors.

**Experimental Section**

**Synthesis of $[Zr_3(\mu_3\text{-}OH)_4(OH)_4(C_{46}H_{34}O_8)]$•10DEF, MFM-133(Zr).** The ligand $H_4TCHB$ was synthesised using the reported procedure.[30] A mixture of $H_4TCHB$ (0.05 g, 0.07 mmol), $ZrCl_4$ (0.049 g, 0.21 mmol) and benzoic acid (1.75 g, 14.3 mmol) was dissolved in DEF (10 mL) using a sonication bath. The resulting solution was heated at 120 °C for 48 h, after which colorless polyhedral crystals were collected by filtration and washed with fresh DEF (3 x 20 mL). Yield: 0.104 g (70%). Anal. Calcd (%) for $C_{95}H_{152}N_{10}O_{26}Zr_3$: C, 53.98; H, 7.17; N, 6.56. Found (%): C, 53.80; H, 7.01; N, 6.25.

**Synthesis of $[Hf_3(\mu_3\text{-}OH)_4(OH)_4(C_{46}H_{34}O_8)]$•9DEF, MFM-133(Hf).** A mixture of $H_4TCHB$ (0.05 g, 0.07 mmol), $HfCl_4$ (0.067 g, 0.21 mmol) and benzoic acid (1.75 g, 14.3 mmol) was dissolved in DEF (10 mL) using a sonication bath. The resulting solution was heated at 120 °C for 48 h, after which colorless polyhedral-shaped crystals were collected by filtration and washed with fresh DMF (3 x 20 mL). Yield: 0.12 g (75%). Anal. Calcd (%) for $C_{91}H_{141}N_9O_{25}Hf_3$: C, 47.59; H, 6.19; N, 5.49. Found (%): C, 47.22; H, 6.14; N, 5.13.

**High Pressure Crystallography**

High pressure experiments were carried out using a locally-assembled Merrill-Basset diamond anvil cell (DAC) [opening angle 80° (4θ), Boehler-Almax anvil type 1A, WC backing plates and 200 μm tungsten gaskets]. A colorless crystal of MFM-133(Zr) or MFM-133(Hf) was loaded into the DAC with a ruby sphere as the pressure calibrant and 4:1 methanol/ethanol as the pressure-transmitting medium (PTM). Diffraction data were recorded using either Mo-Kα radiation ($\lambda$ = 0.71073 Å with microfocus source and focussing mirrors) on an in-house Rigaku Oxford Diffraction SuperNova diffractometer equipped with an Eos CCD detector, or monochromatic synchrotron radiation ($\lambda$ = 0.6889 Å) on a Rigaku Saturn 724+ CCD

diffractometer on Beamline I19 at Diamond Light Source. Diffraction data were processed using the program *CrysAlisPRO* (Version 1.171.37.31).[31] Structures were solved by transferring the fractional coordinates of the atoms as determined at an adjacent pressure and refined using *SHELXTL*-2014.[32] Satisfactory structural refinements were obtained from all datasets. Due to the inherent low completeness of the diffraction data caused by the presence of the diamond anvil cell, restraints were required.

**Supporting Information**

Supporting information is available free of charge on the ACS Publications website. Porosity characterisation for MFM-133(Zr) and MFM-133(Hf); Crystallographic details for high pressure studies. CIF files can be obtained free of charge from the Cambridge Crystallographic Data Centre via www.ccdc.cam.ac.uk/data_request/cif.

**Author Information**

**Corresponding Author**

*A.J.Blake@nottingham.ac.uk

*M.Schroder@manchester.ac.uk

**Notes**

The authors declare that they have no competing financial interests.

**Acknowledgements**

We thank the EPSRC (EP/I011870), ERC (Advanced Grant AdG 226593) and the Universities of Manchester and Nottingham for funding. We are grateful to Diamond Light Source for access to Beamline I19.

**References:**

1. (a) Easun, T. L.; Moreau, F.; Yan, Y.; Yang, S.; Schröder, M. *Chem. Soc. Rev.* **2017**, *46*, 239–274. (b) Carrington, E. J.; Vitórica-Yrezábal, I. J.; Brammer, L. *Acta Cryst., Sect. B* **2014**, *70*, 404–422.
2. (a) Coudert, F.-X. *Chem. Mater.*, **2015**, *27*, 1905–1916. (b) McKellar, S. C.; Moggach, S. A. *Acta Cryst. Sect. B* **2015**, *71*, 587–607.

3. Ortiz, A. U.; Boutin, A.; Gagnon, K. J.; Clearfield, A.; Coudert, F.-X. *J. Am. Chem. Soc.* **2014**, *136*, 11540–11545.
4. Bennett, T. D.; Cheetham, A. K. *Acc. Chem. Res.* **2014**, *47*, 1555–1562.
5. Baughman, R. H.; Stafström, S.; Cui, C.; Dantas, S. O. *Science* **1998**, *279*, 1522–1524.
6. Cairns, A. B.; Goodwin, A. L. *Phys. Chem. Chem. Phys.* **2015**, *17*, 20449–20465.
7. Mariathasan, J. W. E.; Finger, L. W.; Hazen, R. M. *Acta Crystallogr., Sect. B* **1985**, *41*, 179–184.
8. McCann, D. R.; Cartz, L.; Schmunk, R. E.; Harker, Y. D. *J. Appl. Phys.* **1972**, *43*, 1432–1436.
9. Fortes, A. D.; Suard, E.; Knight, K. S. *Science* **2011**, *331*, 742–746.
10. Goodwin, A. L.; Keen, D. A.; Tucker, M. G. *Proc. Natl. Acad. Sci. U.S.A.* **2008**, *105*, 18708–18713.
11. Cairns, A. B.; Thompson, A. L.; Tucker, M. G.; Haines, J.; Goodwin, A. L. *J. Am. Chem. Soc.* **2012**, *134*, 4454–4456.
12. (a) Cai, W.; Katrusiak, A. *Nat. Commun.* **2014**, 5:4337. (b) Cai, W.; Gładysiak, A.; Anioła, M.; Smith, V. J.; Barbour, L. J.; Katrusiak, A. *J. Am. Chem. Soc.* **2015**, *137*, 9296–9301. (c) Yeung, H. H.-M.; Kilmurray, R.; Hobday, C. L.; McKellar, S. C.; Cheetham, A. K.; Allan, D. R.; Moggach, S. A. *Phys. Chem. Chem. Phys.* **2017**, *19*, 3544–3549. (d) Binns, J.; Kamenev, K. V.; Marriott, K. E. R.; McIntyre, G. J.; Moggach, S. A.; Murrie, M.; Parsons, S. *Chem. Commun.* **2016**, *52*, 7486–7489.
13. (a) Baughman, R. H. *Nature* **2003**, *425*, 667. (b) Grima, J. N.; Caruana-Gauci, R. *Nat. Mater.* **2012**, *11*, 565–566.
14. Evans, K.E.; Alderson, A. *Adv. Mater* **2000**, *12*, 617–628.
15. Graham, A. J.; Allan, D. R.; Muszkiewicz, A.; Morrison, C. A.; Moggach, S. A. *Angew. Chem. Int. Ed.* **2011**, *50*, 11138–11141.
16. (a) Spencer, E. C.; Angel, R. J.; Ross, N. L.; Hanson, B. E.; Howard, J. A. K. *J. Am. Chem. Soc.* **2009**, *131*, 4022–4026. (b) Moggach, S. A.; Bennett, T. D.; Cheetham, A. K. *Angew. Chem. Int. Ed.* **2009**, *48*, 7087–7089.
17. (a) Ortiz, A. U.; Boutin, A.; Fuchs, A. H.; Coudert, F.-X. J. *Chem. Phy.* **2013**, *138*, 174703. (b) Grima, J. N.; Attard, D.; Caruana-Gauci, R.; Gatt, R. *Scripta Materialia* **2011**, *65*, 565–568.
18. Serra-Crespo, P.; Dikhtiarenko, A.; Stavitski, E.; Juan-Alcañiz, J.; Kapteijn, F.; Coudert, F.-X.; Gascon, J. *CrystEngComm* **2015**, *17*, 276–280.
19. Zeng, Q.; Wang, K.; Zou, B. *J. Am. Chem. Soc.* **2017**, *139*, 15648–15651.
20. Sarkisov, L.; Martin, R. L.; Haranczyk, M.; Smit, B. *J. Am. Chem. Soc.* **2014**, *136*, 2228–2231.
21. (a) Yan, Y.; Yang, S.; Blake, A. J.; Lewis, W.; Poirier, E.; Barnett, S. A.; Champness, N. R.; Schröder, M. *Chem. Commun.* **2011**, *47*, 9995–9997. (b) Yuan, D.; Zhao, D.; Zhou, H.-C. *Inorg. Chem.* **2011**, *50*, 10528–10530. (c) Deria, P.; Gońez-Gualdroń, D. A.; Bury, W.; Schaef, H. T.; Wang, T. C.; Thallapally, P. K.; Sarjeant, A. A.; Snurr, R. Q.; Hupp, J. T.; Farha, O. M. *J. Am. Chem. Soc.* **2015**, *137*, 13183–13190.
22. (a) Cavka, J. H.; Jakobsen, S.; Olsbye, U.; Guillou, N.; Lamberti, C.; Bordiga, S.; Lillerud, K. P. *J. Am. Chem. Soc.* **2008**, *130*, 13850–13851. (b) Morris, W.; Volosskiy, B.; Demir, S.; Gańdara, F.; McGrier, P. L.; Furukawa, H.; Cascio, D.; Stoddart, J. F.; Yaghi, O. M. *Inorg. Chem.* **2012**, *51*, 6443–6445. (c)

Mondloch, J. E.; Bury, W.; Fairen-Jimenez, D.; Kwon, S.; DeMarco, E. J.; Weston, M. H.; Sarjeant, A. A.; Nguyen, S. T.; Stair, P. C.; Snurr, R. Q.; Farha, O. K.; Hupp, J. T. *J. Am. Chem. Soc.* **2013**, *135*, 10294–10297.

23. (a) Furukawa, H.; Gańdara, F.; Zhang, Y.-B.; Jiang, J.; Queen, W. L.; Hudson, M. R.; Yaghi, O. M. *J. Am. Chem. Soc.* **2014**, *136*, 4369–4381. (b) Zhang, M.; Chen, Y.-P.; Bosch, M.; Gentle III, T.; Wang, K.; Feng, D.; Wang, Z. U.; Zhou, H.-C. *Angew. Chem. Int. Ed.* **2014**, *53*, 815–818.
24. Spek, A. L. *Acta Crystallogr.*, *Sect. D*, **2009**, *65*, 148–155.
25. (a) Tidey, J. P.; Wong, H. L. S.; Schröder, M.; Blake, A. J. *Coord. Chem. Rev.* **2014**, *277–278*, 187–207. (b) Allan, D. R.; Blake, A. J.; Huang, D.; Prior, T. J.; Schröder, M. *Chem. Commun.* **2006**, 4081–4083.
26. The pressure-dependent lattice parameters data were fitted with an empirical expression of the form $l = l_0 + \lambda(p - p_c)^{\nu}$ and the linear compressibilities were determined from the pressure derivative of the above equation: $K(p) = -\frac{1}{l(p)}\lambda\nu(p - p_c)^{\nu-1}$. These calculations were performed with PASCal software: Cliffe, M. J.; Goodwin, A. L. *J. Appl. Crystallogr.* **2012**, *45*, 1321–1329.
27. Li, W.; Probert, M. R.; Kosa, M.; Bennett, T. D.; Thirumurugan, A.; Burwood, R. P.; Parinello, M.; Howard, J. A. K.; Cheetham, A. K. *J. Am. Chem. Soc.* **2012**, *134*, 11940–11943.
28. (a) Birch, F. *Phys. Rev.* **1947**, *71*, 809–824. (b) Sata, N.; Shen, G.; Rivers, M. L.; Sutton, S. R. *Phys. Rev. B* **2002**, *65*, 104114.
29. Hobday, C. L.; Marshall, R. J.; Murphie, C. F.; Sotelo, J.; Richards, T.; Allan, D. R.; Düren, T.; Coudert, F.-X.; Forgan, R. S.; Morrison, C. A.; Moggach, S. A.; Bennett, T. D. *Angew. Chem. Int. Ed.* **2016**, *55*, 2401–2405.
30. Moorthy, J. N.; Natarajan, R.; Venugopalan, P. *J. Org. Chem.* **2005**, *70*, 8568–8571.
31. Agilent Technologies, *CrysAlisPRO* Software system, version 1.171.37.31, Agilent Technologies UK Ltd, Oxford, UK, 2014.
32. Sheldrick, G. M. *Acta Cryst. Sect. C* **2015**, *71*, 3−8.

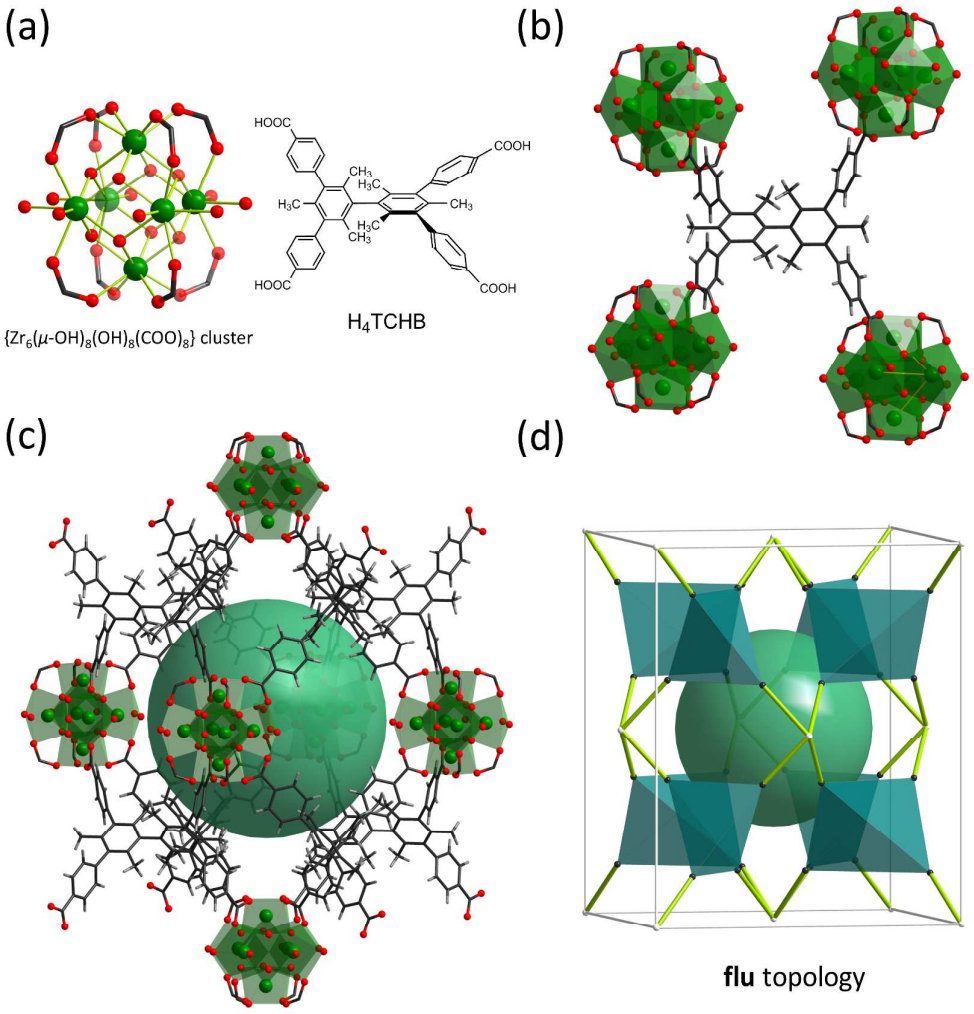


**Figure 1.** The single crystal structure of MFM-133(Zr) at ambient pressure and 120 K. Views of (a) the octahedral $\{Zr_6(\mu\text{-}OH)_8(OH)_8(COO)_8\}$ cluster and $H_4$TCHB; (b) the conformation of $TCHB^{4-}$ units in the framework showing the twisted geometry of the two central mesitylene rings; (c) the octahedral cage constructed from eight $TCHB^{4-}$ units and six $\{Zr_6\}$ clusters; (d) the (4, 8)-connected **flu**-type topology of MFM-133(Zr). Color scheme: Zr, green; O, red; C, black.

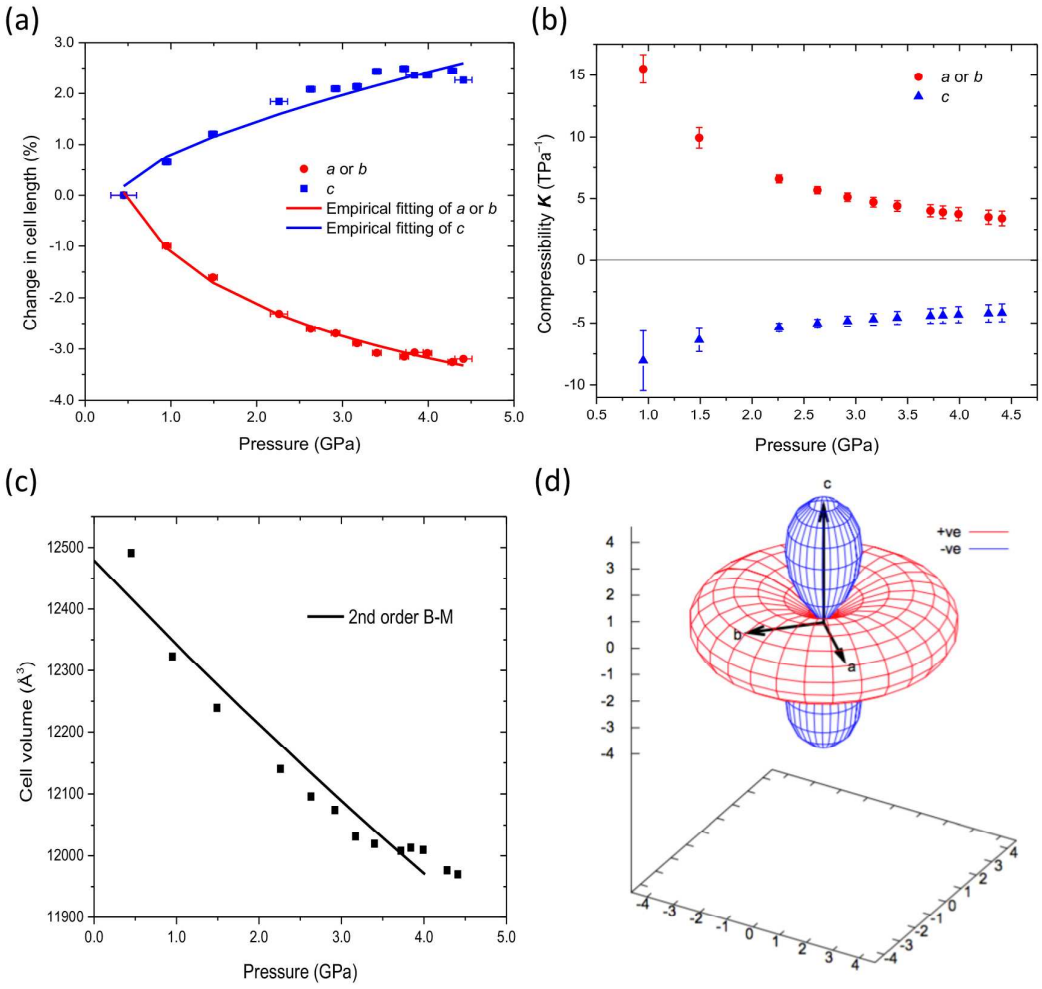


**Figure 2.** High-pressure single-crystal X-ray diffraction experiments for MFM-133(Zr) reveal unusual NLC: (a) the evolution of unit cell lattice parameters as a function of pressure with empirical fitting applied to the experimental data; (b) compressibilities as a function of pressure; (c) variation of unit cell volume with pressure, with the data fitted using a second-order Birch-Murnaghan equation of state; (d) the compressibility indicatrix for MFM-133(Zr). All axes are in units of $TPa^{-1}$.

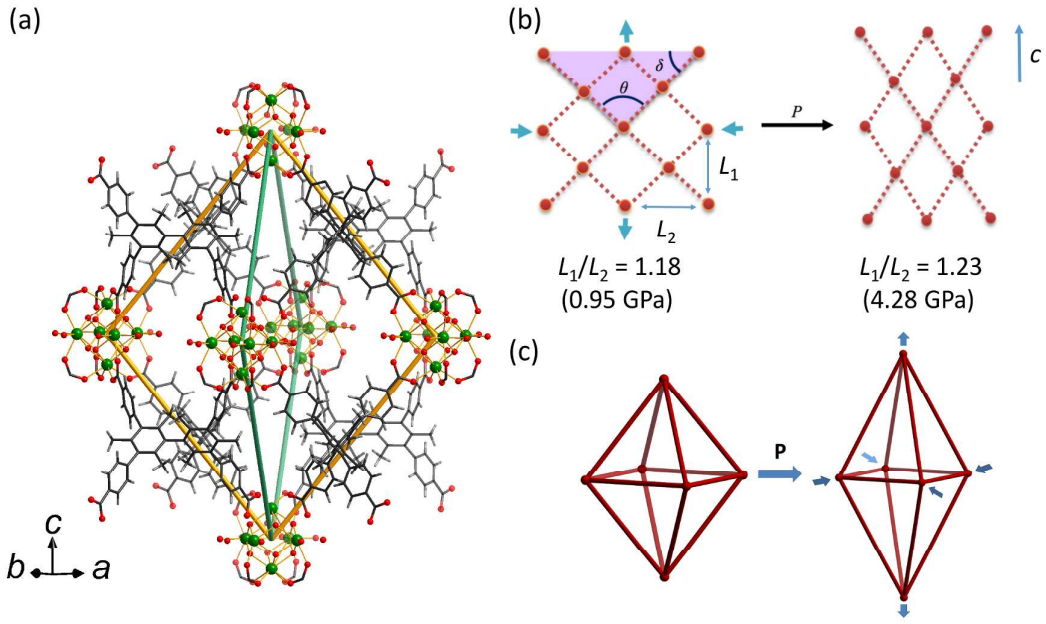


**Figure 3**. Compressibility in MFM-133(Zr). (a) The octahedral cage in MFM-133(Zr) constructed by two identical rhombi (drawn in gold and green) sharing two axial vertices in a perpendicular fashion; (b) simplified representation of the crystal structure of MFM-133(Zr) viewed as the tessellation of the rhombi shown in (a) in two dimensions: {$Zr_6$} clusters are represented as red circles and the organic linkers as dotted lines. The schematic diagram shows the effect of compression on the unit cell dimensions *a* and *c*, as well as the angles θ and δ. The two diagonal axes of the octahedron are defined as $L_1$ and $L_2$; (c) schematic representation of the change of shape of the octahedral cage under compression.

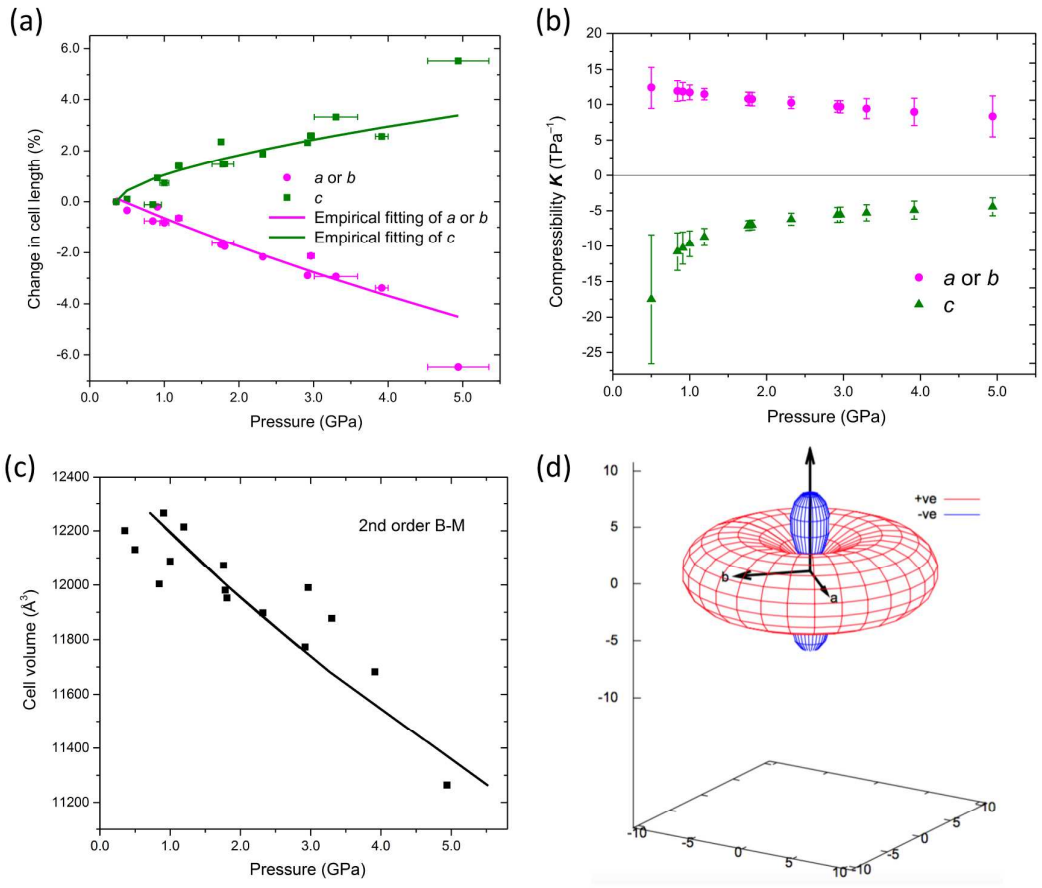


**Figure 4**. NLC in MFM-133(Hf) revealed by high-pressure single-crystal X-ray diffraction: (a) the evolution of unit cell lattice parameters for MFM-133(Hf) as a function of pressure with empirical fits applied to the experimental data; (b) lattice compressibilities as a function of pressure; (c) variation of unit cell volume with pressure with the data fitted using a second-order Birch-Murnaghan equation of state; (d) the compressibility indicatrix for MFM-133(Hf). All axes are in units of $TPa^{-1}$.

**Table of Contents Graphic**